The Effect of Ply Properties in Paperboard Converting Operations: A Way To Increase Formability

Gustav Lindberg (gulindbe@kth.se)

KTH Royal Institute of Technology: Kungliga Tekniska Hogskolan https://orcid.org/0000-0001-5033-7611

Artem Kulachenko

Royal Institute of Technology: Kungliga Tekniska Hogskolan

Research Article

Keywords: tray forming, paperboard, refining energy, multi-ply, non-linear finite elements

Posted Date: February 8th, 2022

DOI: https://doi.org/10.21203/rs.3.rs-1305595/v1

The effect of ply properties in paperboard converting operations: A way to increase formability

Gustav Lindberg*, Artem Kulachenko

Department of Engineering Mechanics, KTH Royal Institute of Technology, Stockholm, Sweden

*Corresponding author: gulindbe@kth.se

Author contribution

Both authors have taken equal responsibility in writing the manuscript. Gustav Lindberg has taken the main responsibility to build the FE models in Ansys and Artem Kulachenko has provided expert guidance in that work. The script for fitting the numerical material model to the tensile tests has been written by Artem Kulachenko prior to this study. Artem Kulachenko has also written the routine for choosing the correct yield surface during the Ansys analysis. The experimental part for this study was done by Gustav Lindberg, and Artem Kulachenko offered expert guidance in that work.

Keywords: tray forming; paperboard; refining energy; multi-ply; non-linear finite elements.

Abstract

This study addresses the question of how the difference in mechanical properties of the individual layers in a multiply commercial paperboard affects the outcome of the tray-forming operation. Two commercially produced paperboards with nearly identical mechanical properties when conventionally tensile tested were considered. These boards are produced on different machines with the same target grammage and density. Despite the similar mechanical properties, their performance in a given tray-forming operation was drastically different, with one of the boards showing an unacceptable failure rate. To investigate the difference seen during converting operations, a detailed multi-ply finite element model was built to simulate the converting operation. The present model considers a critical area of the paperboard known to exhibit failures. To derive the constitutive relations for each ply in the sub-model, both boards were split to single out individual plies which were then tensile tested. Including the properties of individual plies revealed large differences between the boards when it comes to the distribution of the properties in the thickness direction. In particular, the top plies differed to a large extent. This is attributed to the difference in refining energies for the plies. The results from the three-ply sub-model demonstrated the importance of including the multiply structure in the analysis. Weakening of the top ply facing the punch by using lower refining energy considerably increased the risk of failure of the entire board. These results suggest that there is room for optimizing the board performance by adjusting the refining energy at the ply level.

Introduction

The pressure of reducing the use of plastics creates opportunities for the use of paperboard in producing products like plates, food trays, cups, and other containers (Hagman et al. 2017; Rhim 2010; Vishtal and Retulainen 2012). This requires that the board undergoes forming operations. Compared to plastics and sheet metal, paperboard has lower formability. For example, deep drawing of sheet metal is widely used by many industries (Chen and Lin 2007; Reddy, Reddy and Ramanjaneyulu 2019; Rojek et al. 2004). Similarly, plastics are used to form a variety of trays and containers (Gill, Jin and Song 2020; Siracusa et al. 2008). At the same time, the effort to increase the formability of paperboard and improve the processes enabling the forming operation is ongoing, since paperboard is an important part of shifting towards a circular bioeconomy (Wang et al. 2021). As a part of the product development process using paperboard, simulations of the forming operations can be used. With such simulations, the impact of the paperboard properties on the risk of failure during forming operations can be assessed.

The current study is a continuation of the work performed in Lindberg and Kulachenko (2021), where the tray forming operation was simulated using an implicit non-linear finite element (FE) model using a single-ply approach. In contrast to the previous study, where the difference between the boards can be seen already on the sheet level, the boards considered here have similar properties, but still show of differences in performance. The paperboards are produced on two separate board machines, and are herein called Board A and Board B. It is desirable that both machines can produce identical paperboard, i.e. that Board A and Board B are identical. At the time of the study, however, only Board B had no reported problems at the customer end. In Lindberg and Kulachenko (2021), the tensile tests showed observable differences between the two boards on the sheet level, with Board B having higher stress and strain to failure in the paperboard machine direction (MD) and the cross-machine direction (CD), but somewhat lower stress and strain to failure in the 45-direction. The FE-model in that study predicted that the observed differences on the sheet level can explain the performance degradation in Board A. The model was also capable to predict the position of the failure.

The current study was initiated after the refining energies for Board B were modified in the process development trials which eliminated the differences between the two boards in the tensile tests. I.e., now Board B only had slightly larger strength and strain to failure compared to Board A, such that the difference no longer had a significant role. Board A remained unchanged. Despite the modified refining energies, no problems were reported for this new version of Board B. This raised the question of whether there is any other difference that can explain the degradation in performance of Board A. To advance the investigation, the current study focused on the individual plies of the boards and their effect on the

paperboard behavior in the tray forming operation. For this, a three-ply FE sub-model was built where the plies were modeled with their individual material properties and thicknesses. The model is a sub-model of the model in Lindberg and Kulachenko (2021). The sub-model is simulating the area constituting the critical lower corner in the tray forming process, see Fig. 1. As a part of obtaining the numerical material models for the plies, the two boards were split into their plies, and then tensile tested in MD, CD and the 45-direction. Already at that stage, differences were discovered, where foremost the top plies of the two boards had large differences in the tensile test curves. The Board A top ply was considerably weaker than the Board B top ply, and at the same time the Board A bottom ply was very stiff. This difference appeared due to various refining energies used for the pulps. For example, the top ply of Board A had much lower refining energy than its bottom ply, meanwhile, the Board B top and bottom plies had very balanced refining energies, i.e. the outer plies had about the same level of refining energy.

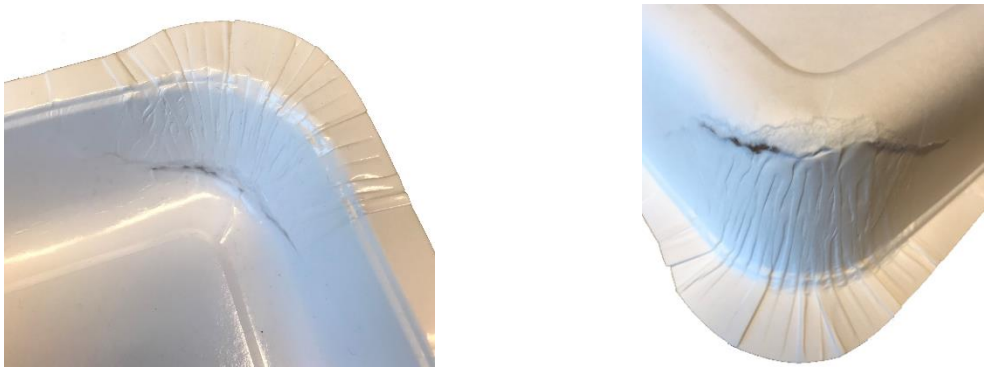

Fig. 1 - The failed corner during the converting operation using Board A (Lindberg and Kulachenko 2021).

The effect of the refining energy on cellulose material is a very well investigated research field (Jele, Lekha and Sithole 2021). The refining energy affects the number of contacts between the fibers, which affects the tensile properties of paperboard as well as reinforcing the fiber joints in the network due to added fine content (Motamedian, Halilovic E and Kulachenko 2019). Most importantly, refining energy is one of the tools which the manufacturer can leverage. Hence, its impact on the forming operation through the changes to the ply properties is of utmost interest. During converting operations, wrinkling of the paperboard in specific locations, such as corners, is a necessary part of the forming process. In experiments, it has been seen that refined fibers make significantly higher wrinkle strength, but at the same time that high refining energy lowers the 3D formability of paperboard (Hauptmann et al. 2015). To increase the formability, it has been suggested that softwood pulp could partially replace the more common birch kraft in paperboards designed for 3D forming applications (Laukala et al. 2019). It has also been suggested that adding gelatin and agar to the pulp could increase the formability of the final paperboard (Vishtal et al. 2015).

Simulations of deep drawing and tray forming of paperboard have been used previously (Awais et al. 2017; Linvill, Wallmeier and Östlund 2017; Wallmeier et al. 2015), with different numerical approaches and objectives. However, the current approach with a multi-ply model for large deformation of paperboard in converting operations has never been done before. With this multi-ply model, we show how the formability can be improved for a commercially produced paperboard.

The advances with the current study are:

a) the inclusions of the individual ply properties in the modeling of converting operations;
b) using a sub-modelling approach allowing a more detailed investigation of the critical areas in tray forming;
c) presenting the evidence of the importance of the multiply structure for the formability of the boards.

Materials and methods

The approach in this study was to perform tensile tests of the split and unsplit paperboards, followed by numerical simulations of the critical lower corner of the tray. With the tensile tests of split paperboards, we derived constitutive relations for each ply and assigned them to the numerical model.

The geometry of the tray

In Fig. 2 the paperboard blank is shown as it is prepared by the tray manufacturer for the forming operation. The blank is laminated with a polymer that is extruded over the blank since the tray must withstand moisture during usage. The creasing pattern containing 30 creases in each corner has been impressed on the paperboard to facilitate the formation of folds at the corners. The grammage of the paperboards was 330 g/m^2 and the thickness including the thin (30µm) and compliant PET (polyethene terephthalate) coating was 0.470 mm. The PET coating is applied on the top ply, i.e. the ply that meets the punch in the tray forming operation. The herein called bottom ply meets the die in the forming operation.

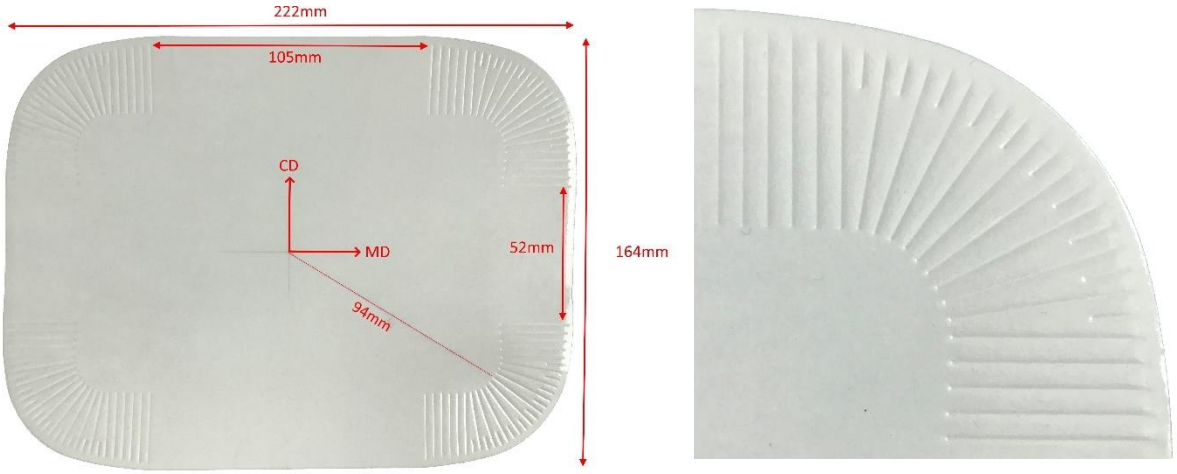

Fig. 2 - The paperboard blank before forming operation. a) The full blank with dimensions and b) close-up of the creases (Lindberg and Kulachenko 2021).

Fig. 3 shows the studied tray after a successful forming operation, that is, without detectable failure. The linear dimensions of the formed tray are 185x125x25 mm.

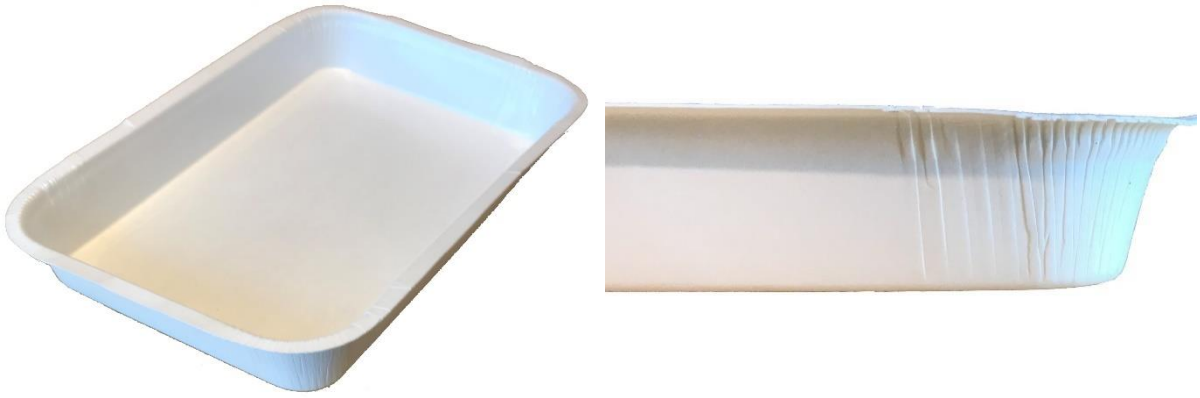

Fig. 3 - The studied tray after a successful forming operation. In a) seen slightly from above and in b) seen from the side (Lindberg and Kulachenko 2021).

Board A is a four-ply paperboard, and Board B is a three-ply paperboard. The two middle plies for Board A are identical in their mechanical properties and were treated as one single ply. Hence, both Board A and Board B were simulated as three-ply paperboards.

Tensile tests and thickness measurements

For this study, uniaxial tensile tests of the full boards and the individual plies were conducted at KTH Royal Technical Institute. To avoid laboratory sheets, Board A and Board B were split, i.e. the plies come from commercially produced paperboard (Inverform). The two boards were split using a Fortuna Splitting Machine for paperboard, model AB 320P. The paperboard is fed through two rolls, and a band knife is adjusted to split the board into the desired thickness, as illustrated in Fig. 4.

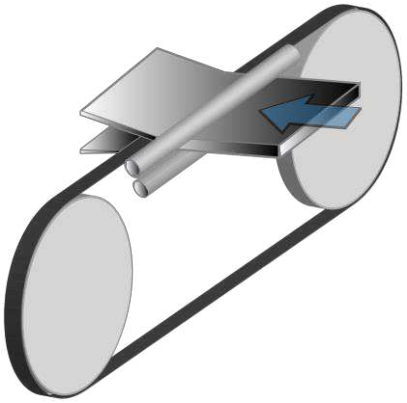

Fig. 4 – Illustration of the splitting process using a Fortuna Splitting Machine.

The tensile tests were prepared by cutting the test specimens into the dimension of 40x10 mm. Specimens were created to be aligned with the paperboard MD, CD, and 45-direction. The specimens were stored for 48 hours in a climate-controlled room holding 50% RH and 25°C (ISO conditions). This procedure was used for both the unsplit boards and the individual plies. The tensile test machine was a Zwick Roell Z1.0, with an optical tracking system of the deformation of the test specimen. The specimen was placed in specially designed grippers which are mounted on the robotic arms pulling the specimen apart. In order to exclude the factor of slippage which may occur between the grippers and the specimen, the optical tracking system was used to register the deformation of the specimen. In Fig. 5 an ongoing tensile test is shown, where the red squares track the spots located on the surface of the test specimen.

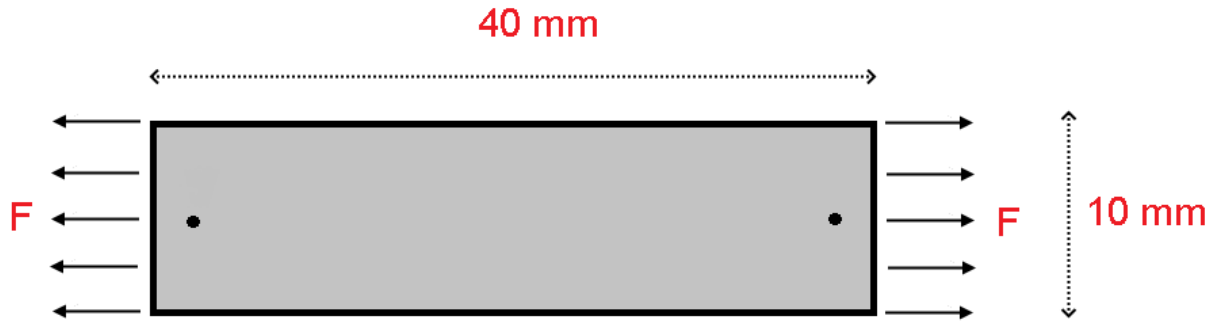

Fig. 5 – Sketch showing the tensile test, with the force F [N] pulling the specimen, and the round markers which are being tracked by the optical tracking system**.**

The output from the tensile tests is displacement-force curves. To determine the stress curve, the thickness of the plies had to be measured. The measurements were performed using an STFI Thickness Tester M201, which can be seen in Fig. 6. The paperboard is continuously fed through the machine, and a thickness profile is measured. This procedure follows the standard SCAN-P88:01 (Scandinavian Pulp, Paper and Board testing committee. SCAN-P 88:01 2001).

a) b) c)

Fig. 6 – The STFI Thickness Tester M201 used to measure the thickness of the plies. In a) and b) the instrument shown before the paperboard is being fed through it, and in c) during thickness measurements.

Table 1 shows the results from the thickness measurements of the individual plies. If the mean thickness for the plies is summarized for each board, the mean thickness for Board A is 444 µm, and for Board B 451 µm. The target thickness for the un-coated paperboards was 440 µm, so the results deviated by 0.9% and 2.5% respectively from the expected.

Table 1 – Results from the thickness measurements of the individual plies.

Ply	Mean thickness [µm]	Thickness standard deviation [µm]	Density [kg/m^3]
Board A top	89	12	830
Board A middle	238*	15	680
Board A bottom	117	8	830
Board B top	103	10	835
Board B middle	239	12	660
Board B bottom	109	9	835

*Consists of two plies with similar properties.

Fig. 7 shows the results of the uniaxial tensile tests performed for the unsplit boards. The tensile tests are performed under ISO standard conditions in three in-plane directions, MD, CD and 45°. Five tests were performed in each direction. The tests in the three in-plane directions enable accurate calibration of the material properties (Alzweighi et al. 2021). As seen in Fig. 7 and Table 2 the two boards have similar behavior. Board B allows for slightly higher strain and stress to failure. However, when the results from the individual plies are studied, they reveal greater differences between the boards, especially in the top plies. This means that using the unsplit samples does not disclose relevant differences which can explain a drastic change in performance.

Table 2 – Mean and standard deviation for the tensile test of the full boards in Fig. 7.

	Board A			Board B		
Direction	MD	45	CD	MD	45	CD
Tensile stress Mean value [MPa]	49	34	26	57	38	28
Tensile stress STD [MPa]	1.9	1.7	1.1	2.3	1.1	1.1

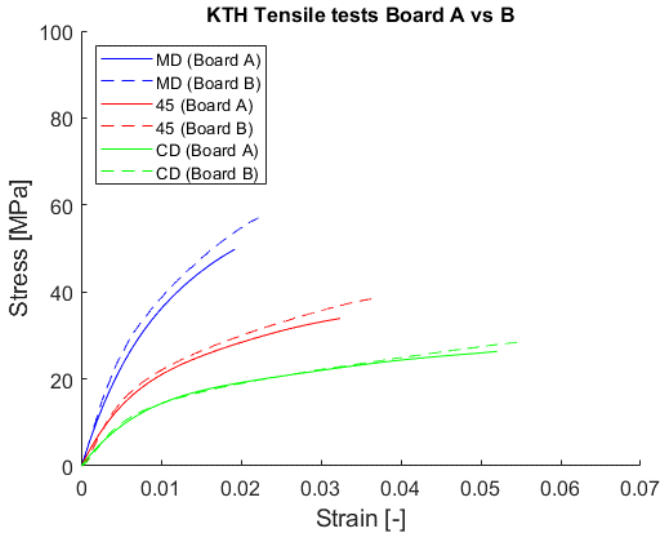

Fig. 7 – The tensile tests of the unsplit commercially produced Board A and Board B.

Fig. 8 shows the uniaxial tensile tests of the individual plies. Here, three tests were performed in each of the three in-plane directions for each ply. As seen, the Board A top ply has a lower strain and stress to failure in all three test directions (MD, 45 and CD) compared to the Board B top ply. The middle plies for both boards have similar behavior and have rather low strain and stress to failure. This is due to the relatively low refining energies for the middle plies. For the bottom ply, Board A has greater stress to failure, but Board B shows a slightly larger strain to failure. Due to a complex load case including both tensile and bending loads, this difference may have significance in the tray forming process despite the fact that the difference is not reflected in the pure tensile tests of the entire boards (Fig. 7).

By comparing Fig. 7 and Fig. 8, it is noticeable that the failure strain in, foremost, the 45-direction is higher for the full boards (Fig. 7), than for any individual ply (Fig. 8). This can be explained by two factors. First, certain damage can be introduced as the paperboards are split, which would affect the tensile tests of the individual plies. Another reason could be that a size effect exists through the thickness of paperboard in the same way as it exists for the width (Hagman and Nygårds 2012; Hristopulos and Uesaka 2004; Kulachenko and Uesaka 2012), which shows that increasing the width of test specimen from small size initially increases the strength and strain to failure before it starts to decrees at larger sizes. In Appendix (Fig. 19), the tensile test results for each ply in their respective direction are shown together with the tensile tests of the full board to facilitate the comparison.

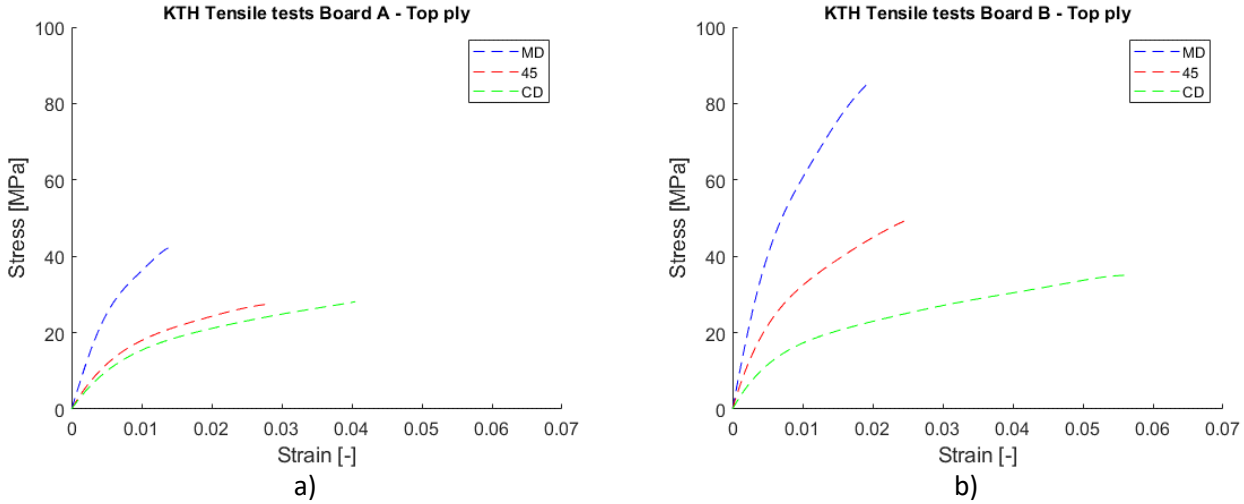

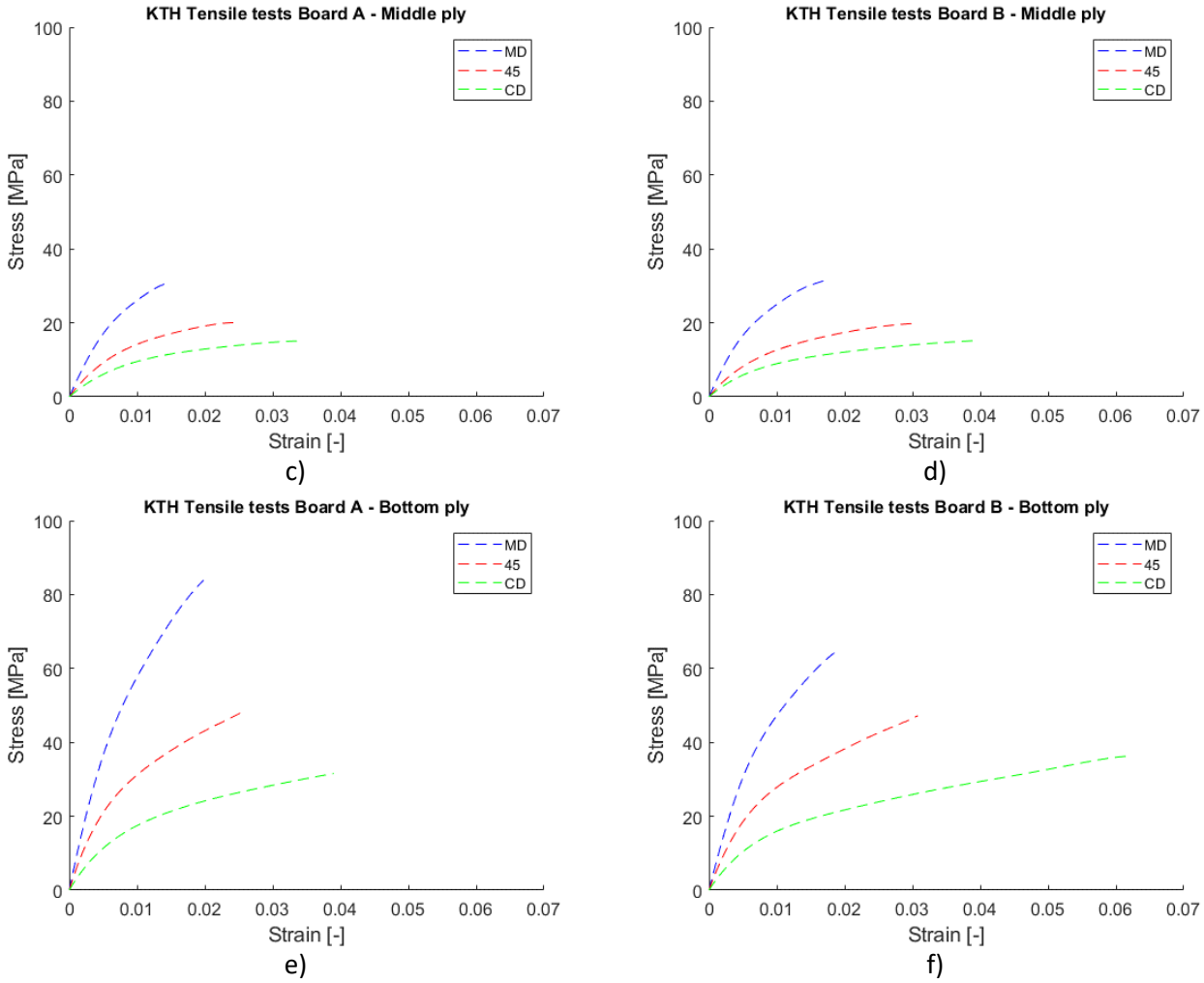

Fig. 8 – The tensile tests of the individual plies from the two split commercially produced paperboards.

Fiber Characterization

In addition to the above-described experiments, a quantification of the geometric fiber properties was done during this study. For this, the tool PulpEye was used, which measures the fiber properties in the pulp before going into the paperboard machine. The results from these measurements are shown in Appendix. Note that the PulpEye measurements were done on a different occasion than for the production of the paperboards used in the above-described experiments, but the settings for the refining energies were the same.

Material description

Paperboard is an anisotropic material, which may be approximated as an orthotropic material. The material shows different responses in tension and compression. The source for the input data was the physical tensile tests of the two paperboard types and their plies considered in this study, see Fig. 8. Paperboard exhibit a reduction in yield limit and strength in compression compared to the corresponding values in tension (Fellers et al. 1980; Xia, Boyce and Parks 2002). This is taken into account by assuming the yield stress in compression is 70% of that in tension. For the failure evaluation, the compressive strength is reduced by 50% from the tensile value. The chosen values for yield and failure stress levels in compression are based on the reported values in Xia, Boyce and Parks (2002). It is important to note that the failures addressed in this study are exclusively tensile. However, as the failure surface is continuous the compressive part affects it too.

Elastic material properties

In the following theory, the principal material directions MD, CD and ZD are described with indices 1, 2 and 3, respectively. The elastic part of the paperboard is described using Hooke's law $\boldsymbol{\varepsilon} = \boldsymbol{C}\boldsymbol{\sigma}$. For an orthotropic material the full expression reads

$$\begin{bmatrix} \varepsilon_{11} \\ \varepsilon_{22} \\ \varepsilon_{33} \\ \varepsilon_{23} \\ \varepsilon_{31} \\ \varepsilon_{12} \end{bmatrix} = \begin{bmatrix} \frac{1}{E_1} & \frac{-\nu_{21}}{E_2} & \frac{-\nu_{31}}{E_3} & 0 & 0 & 0 \\ \frac{-\nu_{12}}{E_1} & \frac{1}{E_2} & \frac{-\nu_{32}}{E_3} & 0 & 0 & 0 \\ \frac{-\nu_{13}}{E_1} & \frac{-\nu_{23}}{E_2} & \frac{1}{E_3} & 0 & 0 & 0 \\ 0 & 0 & 0 & \frac{1}{2G_{23}} & 0 & 0 \\ 0 & 0 & 0 & 0 & \frac{1}{2G_{31}} & 0 \\ 0 & 0 & 0 & 0 & 0 & \frac{1}{2G_{12}} \end{bmatrix} \begin{bmatrix} \sigma_{11} \\ \sigma_{22} \\ \sigma_{33} \\ \sigma_{23} \\ \sigma_{31} \\ \sigma_{12} \end{bmatrix}. \tag{1}$$

The paperboards are modeled with 3D shells with plane stress assumption. In the case of plane stress, the expression in Equation (1) reduces to

$$\begin{bmatrix} \varepsilon_{11} \\ \varepsilon_{22} \\ \varepsilon_{12} \end{bmatrix} = \begin{bmatrix} \frac{1}{E_x} & \frac{-\nu_{21}}{E_y} & 0 \\ \frac{-\nu_{12}}{E_x} & \frac{1}{E_y} & 0 \\ 0 & 0 & \frac{1}{2G_{12}} \end{bmatrix} \begin{bmatrix} \sigma_{11} \\ \sigma_{22} \\ \sigma_{12} \end{bmatrix}. \tag{2}$$

The two in-plane values for Young's modulus E_i in Equation (2) are determined by the fitting procedure, and the in-plane shear modulus G_{12} and Poisson's ratio ν_{12} are then calculated using the two separate relations for commercially produced papers (Baum, Habeger Jr and Fleischman Jr 1982)

$$G_{12} = \frac{\sqrt{E_1 E_2}}{2\left(1+\sqrt{\nu_{12}\nu_{21}}\right)} \quad \text{and} \quad \sqrt{\nu_{12}\nu_{21}} = 0.293. \tag{3}$$

Equation (3) along with the symmetry condition of the compliance matrix, giving $\nu_{21}/E_2 = \nu_{12}/E_1$, give the in-plane elastic material parameters which are listed in Table 3.

The out-of-plane strain ε_{33} can be derived as $\varepsilon_{33} = \frac{-\nu_{13}}{E_1}\sigma_{11} - \frac{\nu_{23}}{E_2}\sigma_{22}$ as given by Equation (1) with $\sigma_{zz} = 0$, but requires estimations of the Poisson's ratios ν_{31} and ν_{23}.

Table 3 – The elastic material properties for each ply.

Ply	Young's modulus E_1 and E_2 [MPa]	Shear modulus G_{12} [MPa]	Poisson's ratio* ν_{12} [-]
Board A Top	5790, 2599	1130	0.45
Board B Top	9590, 3030	3070	0.52
Board A Middle	3930, 1540	980	0.47
Board B Middle	3940, 1500	860	0.47
Board A Bottom	8600, 2863	2970	0.51
Board B Bottom	7030, 2670	2330	0.48

* ν_{21} is determined from the above parameters due to the symmetry of the stiffness matrix

Hardening model

Plasticity in paperboard has been modeled in many different studies (Alajami, Li and Simon 2018; Bedzra et al. 2019; Harrysson and Ristinmaa 2008; Li et al. 2016; Robertsson et al. 2018; Tjahjanto, Girlanda and Östlund 2015; Xia, Boyce and Parks 2002). The evolution of the plastic strains in the current study is described using Hill's plasticity (Hill 1948), which is suitable for composites and a common way to model plasticity for orthotropic composite such as paperboard. Hill's plasticity is defined as

$$\begin{aligned} f(\sigma,\sigma_f) &= F(\sigma_{22}-\sigma_{33})^2 + G(\sigma_{33}-\sigma_{11})^2 + H(\sigma_{11}-\sigma_{22})^2 \\ &+2L\sigma_{23}^2 + 2M\sigma_{31}^2 + 2N\sigma_{12}^2 - \sigma_y{}^2 = 0 \end{aligned} \quad (4)$$

where F, G, H, L, M and N are defined as

$$\begin{aligned} &F = \frac{1}{2}\left(\frac{1}{R_{12}^2}+\frac{1}{R_{33}^2}-\frac{1}{R_{22}^2}\right); \quad G = \frac{1}{2}\left(\frac{1}{R_{33}^2}+\frac{1}{R_{11}^2}-\frac{1}{R_{22}^2}\right); \quad H = \frac{1}{2}\left(\frac{1}{R_{11}^2}+\frac{1}{R_{22}^2}-\frac{1}{R_{33}^2}\right); \\ &L = \frac{3}{2}\left(\frac{1}{R_{23}^2}\right); \quad M = \frac{3}{2}\left(\frac{1}{R_{13}^2}\right); \quad N = \frac{3}{2}\left(\frac{1}{R_{12}^2}\right). \end{aligned} \quad (5)$$

The Hill's parameters R_{ij} in Equation (5) are defined as

$$R_{11} = \frac{\sigma_{11}{}^y}{\sigma_y}; \quad R_{22} = \frac{\sigma_{22}{}^y}{\sigma_y}; \quad R_{33} = \frac{\sigma_{33}{}^y}{\sigma_y}; \quad R_{12} = \sqrt{3}\frac{\sigma_{12}{}^y}{\sigma_y}; \quad R_{23} = \sqrt{3}\frac{\sigma_{23}{}^y}{\sigma_y}; \quad R_{13} = \sqrt{3}\frac{\sigma_{13}{}^y}{\sigma_y}, \quad (6)$$

and determine the shape of the yield surface, which initial size is determined by the initial yield stresses $\sigma_{ij}{}^y$ and the isotropic yield stress σ_y. The material parameters in Equation (6) are found with the previously mentioned fitting procedure. The stress-strain curve measured in the CD is used as a master curve for the multilinear hardening and the rest of the parameters are fitted in Matlab using the *fmincon*-function to minimize the error between the measured and the calculated tensile test curves. The paperboard is modeled to yield at $R_p = 0.0001$, i.e. the initial yield stress is in this study the stress giving a permanent deformation of 0.01% strain. Such a low value is required to get a good fit between the experimental and the numerical tensile test curves. The quality of the fit is shown in Appendix Fig. 18 for all six plies. The curves on the compressive side are only from the numerical tests since no data is given from experiments. In compression, the two paperboards have a 30% reduction of the yield stress and a 50% reduction of the ultimate stress compared to the tensional side, which renders in the curves on the compressive side in Fig. 18.

The modeled difference in tension and compression for the paperboard plies render in two yield surfaces per ply, one for compression and one for tension. The surface that applies for the current point is

determined by the sign of hydrostatic stress. More about the used hardening model is found in Lindberg and Kulachenko (2021). In Table 4, the complete set of parameters for Hill's plasticity used in this study is presented for all plies. Note that the fit of R_{33} is important even though plane stress is approximated, since R_{33} influences the shape of the yield surface in the MD-CD plane.

Table 4 – The Hill parameters for each ply

Ply	R_{11} [-]	R_{22} [-]	R_{33} [-]	R_{12} [-]	R_{23} [-]	R_{13} [-]
Board A Top	1.913	1.0	1.051	1.104	1.0	1.0
Board B Top	2.809	1.0	1.394	1.723	1.0	1.0
Board A Middle	2.216	1.0	1.222	1.375	1.0	1.0
Board B Middle	2.244	1.0	1.222	1.348	1.0	1.0
Board A Bottom	2.665	1.0	1.299	1.597	1.0	1.0
Board B Bottom	2.409	1.0	1.271	1.611	1.0	1.0

Failure evaluation

Failure is not included in the numerical model but is evaluated as a part of the post-processing of the final results using the Tsai-Wu stress failure criterion (Tsai and Wu 1971). For plane stress, it reads (Li et al. 2017; Suhling et al. 1985)

$$\sigma_{TW} = F_1\sigma_{11} + F_2\sigma_{22} + F_{11}\sigma_{11}^{\ 2} + F_{22}\sigma_{22}^{\ 2} + 2F_{12}\sigma_{11}\sigma_{22} + F_{66}\sigma_{12}^{\ 2} < 1, \tag{7}$$

where F_i and F_{ij} are defined as

$$\begin{aligned} &F_1 = \frac{1}{\sigma_{11}^t} - \frac{1}{\sigma_{11}^c};\quad F_2 = \frac{1}{\sigma_{22}^t} - \frac{1}{\sigma_{22}^c};\quad F_{11} = \frac{1}{\sigma_{11}^{\ t}\sigma_{11}^c};\\ &F_{22} = \frac{1}{\sigma_{22}^{\ t}\sigma_{22}^c};\quad F_{66} = \frac{1}{(\sigma_{12}^t)^2};\quad F_{12} = k\sqrt{F_{11}F_{22}}, \end{aligned} \tag{8}$$

and the indices "t" and "c" are for ultimate tensile stress and ultimate compressive stress respectively. In Equation (8), F_{12} and the in-plane ultimate shear stress $\sigma_{12}^{\ t}$ require some extra attention. These cannot be directly determined from tensile and compressive tests and require shear testing where the failure envelope is studied. For the current study, no such data is given for the two paperboards. Some estimations from the literature are required. For F_{12} the constant k is chosen as $k = -0.5$, which is suitable for most composites (Li et al. 2017; Tsai 1984). In Li et al., for the interested reader, F_{12} is analyzed not only for closed failure surfaces but also for open surfaces. The ultimate shear stress σ_{12}^t in Equation (8) may be estimated by using the geometrical mean of the tensile strength values in MD and CD, as done by Fellers (Fellers, Westerlind and De Ruvo 1983) for evaluation of the compressive modes. This study utilizes the geometrical mean for the tensile modes as

$$\sigma_{12}^t = \sqrt{\sigma_{11}^t\sigma_{22}^t}. \tag{9}$$

In Table 5 the material parameters for the failure evaluation are listed, which are given by the expression in Equation (8) along with the end value of the MD and CD curves in Fig. 8, i.e. the tensile stresses in MD and CD for each ply.

Table 5 – The Tsai-Wu parameters for the plies.

Ply	F_1 [1/MPa]	F_2 [1/MPa]	F_{11} [1/MPa^2]	F_{22} [1/MPa^2]	F_{66} [1/MPa^2]	F_{12} [1/MPa]
Board A Top	-0.0235	-0.0356	0.0011	0.0025	0.0008	-0.0008
Board B Top	0.0352	0.0857	-0.0003	-0.0016	0.0003	-0.0003
Board A Middle	-0.0325	-0.0662	0.0021	0.0088	0.0022	-0.0022
Board B Middle	-0.0318	-0.0657	0.0020	0.0086	0.0021	-0.0021
Board A Bottom	-0.0120	-0.0318	0.0003	0.0020	0.0004	-0.0004
Board B Bottom	-0.0154	-0.0276	0.0005	0.0015	0.0004	-0.0004

Numerical Model

The numerical model developed and used for this study is a sub-model of the model used in Lindberg and Kulachenko (2021), where the lower critical area was successfully identified in the simulations of the full tray forming operation. The simulations in this study were performed with the finite element solver Ansys 2019R1 in a quasi-static regime using an implicit time-integration method. Due to the symmetry, a quarter model is simulated, as seen in Fig. 9. Initially, the blank is located so that the MD is parallel with the global x-axis and CD with the global y-axis. As the simulation starts, the punch presses the blank into the die and forms the tray.

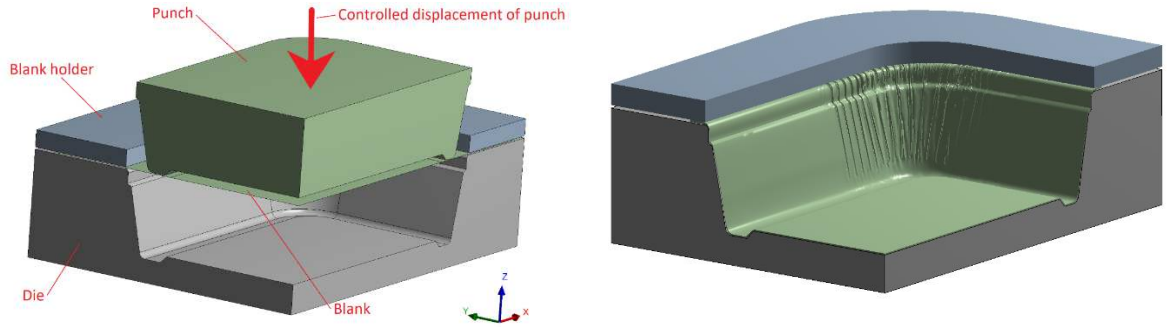

Fig. 9 – The quarter model used in the finite element simulation in Lindberg and Kulachenko (2021). In a) the setup of the model, and in b) the formed tray at the end of the simulation.

The most critical area during the tray forming operation is the lower corner where the tray has been seen to fail during the forming operation (see Fig. 1). In order to resolve this part better with the simulation tools, a detailed sub-model was constructed which allowed: a) to use finer mesh density allowing to capture the strain gradients more accurately and b) resolve the individual plies. The area of the sub-model is about 1.3 cm^2 and is seen in Fig. 10a. In Fig. 10b) the three parts included in the sub-model simulation are viewed: the sub-section of the blank, the die, and the punch.

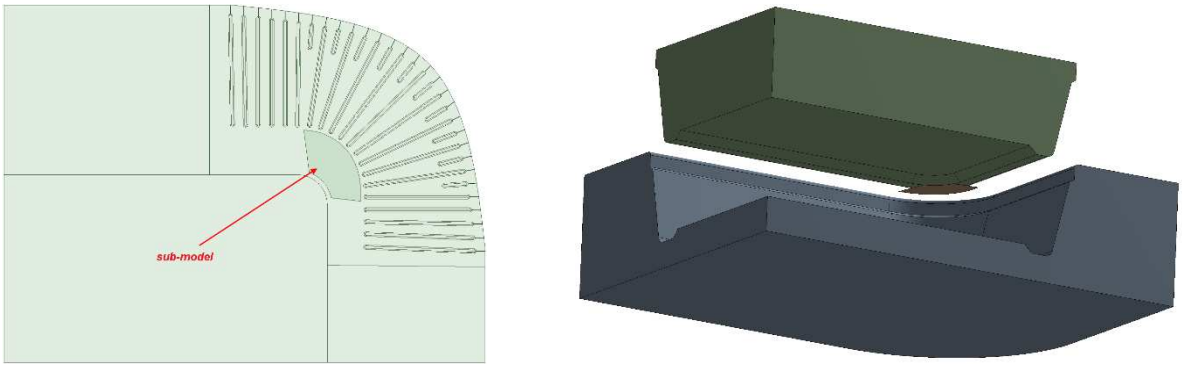

Fig. 10 – The sub-model of the critical lower corner, in a) demonstrated in global model and in b) the full geometry of the sub-model

On the edges of the sub-model, the displacement and rotations from the global model are mapped onto the sub-model (see Fig. 11). I.e., the edges of the sub-model will deform in the same way as the corresponding locations deform in the global model. The remaining part of the sub-model is free to deform and will be influenced by, partly, the mapped boundary conditions on the edges, and mainly by the contact with the punch and, in the end, the contact with the die.

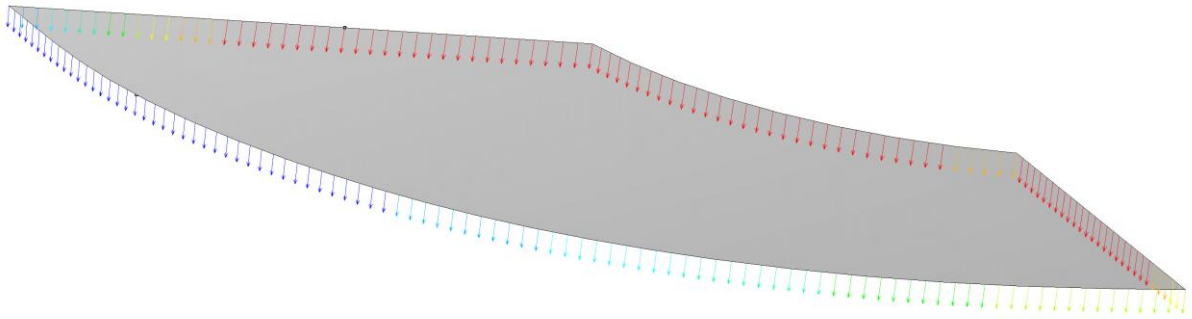

Fig. 11 – Demonstration of the mapped edge boundary conditions, here showing the mapped displacements.

Results three-ply sub-model

Verification of three-ply model

For each of the total six plies, a non-linear orthotropic numerical material model is developed and fitted to the tensile tests of the individual tensile tests shown in Fig. 8. The stress-strain curves in a numerical tensile test are fitted to the actual test curves in an iterative process where the material parameters in the numerical model are changed until the fit between the numerical and actual tensile test curves is sufficient. The final fit between the ply tensile tests and the fitted material models are, as previously mentioned, shown in Appendix (Fig. 18).

To verify the three-ply sub-model, the tensile tests of the full boards (Fig. 7) are compared to numerical tensile tests of a three-ply test specimen. I.e., the numerical test specimen has three different material models through the thickness, and each of the three plies has its individual thickness (see Table 1). The results are shown in Fig. 12.

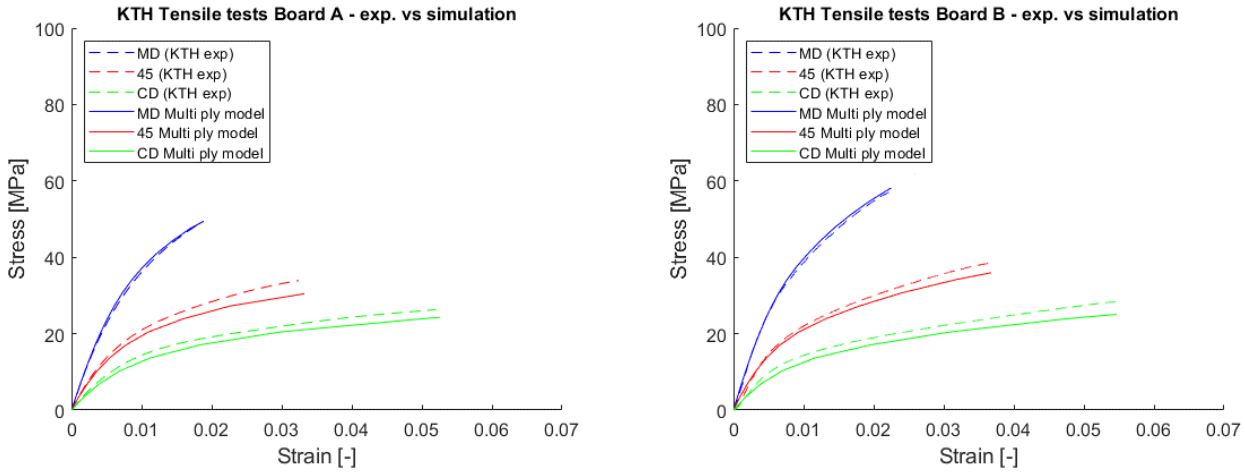

a) b)

Fig. 12 – The tensile tests compared with the numerical tensile tests of the three-ply model with individual thickness and material models for each ply. Note that damage is not included in the numerical models, i.e. the numerical tests were stopped when the actual strain-to-failure was researched.

As seen in Fig. 12, the experimental tensile tests and the numerical tensile tests agree well. Some differences, namely, underestimation of response from the multiply structure can be attributed to the damage introduced by the splitting process as well as the size effects mentioned early when none of the plies surpassed the strain to failure of the entire board.

Results from the 3-ply sub-model

In Fig. 13 the deformed three-ply sub-model of the lower corner is seen at the end of the simulation, i.e. when the punch has pressed the paperboard down to the bottom of the die.

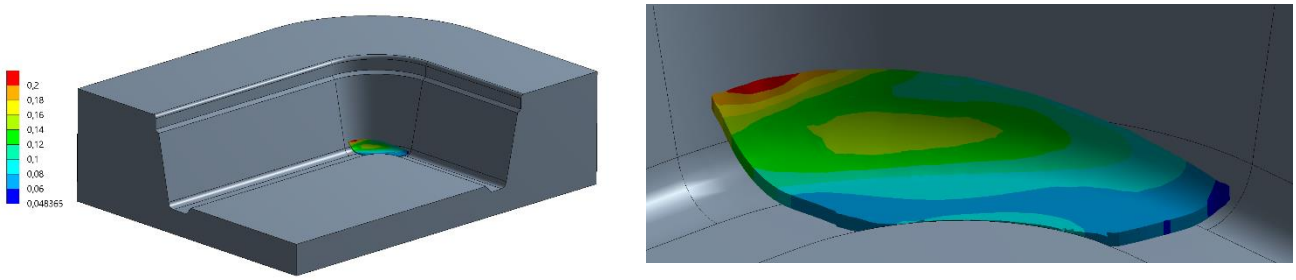

a) b)

Fig. 13 – The sub-model at end of the simulation. In a) the position of the sub-model in the die is seen, and in b) a close-up of the sub-model at the end of the simulation showing the total equivalent strain for the middle ply for Board A.

From the FE-models, we will first focus on the contribution to the load-bearing capacity by each ply. As the stress develops non-uniformly through the deformation process, we for each stress and strain quantity, chose to consider an evolution of the average stress and strain over the sub-model. Stresses and strains are calculated at the integration points. The values are then extrapolated to the nodes of the current element. As one node belongs to several elements, the value in the current node is an average of the extrapolated values from the integration points of the coinciding elements. Then, in turn, the average values of all nodes over the sub-model are used in the evaluation of the sub-model.

In Fig. 14 the total equivalent average strain of the section is shown. The values have been normalized by the highest value occurring for the respective board, which for both boards are the strain level in the

bottom ply at the end of the forming operation. As seen, the bottom ply experiences the highest strain throughout the forming operation, and the middle ply experience roughly 60% of that strain. For the strain in the top ply, there is a difference between the boards. For Board A, the strain level is, in relation to the strain in the bottom ply, higher than for Board B. This is natural, since the Board A top ply is more compliant in comparison to its bottom ply, and hence exhibits greater strain. The absolute values of the strain levels in the bottom plies are high, about 10% in the CD and 3% in MD for Board A, and 8 % in CD and 3% in MD for Board B. Even though locally, much higher strains can exist than what is observed in a standard tensile test (Brandberg and Kulachenko 2020; Hagman and Nygårds 2012), these values are high. A possible contribution to that is not including the delamination in the model which can potentially decrease the strain in the critical area. Despite that, the relative difference between the board is still informative and is used in the discussion.

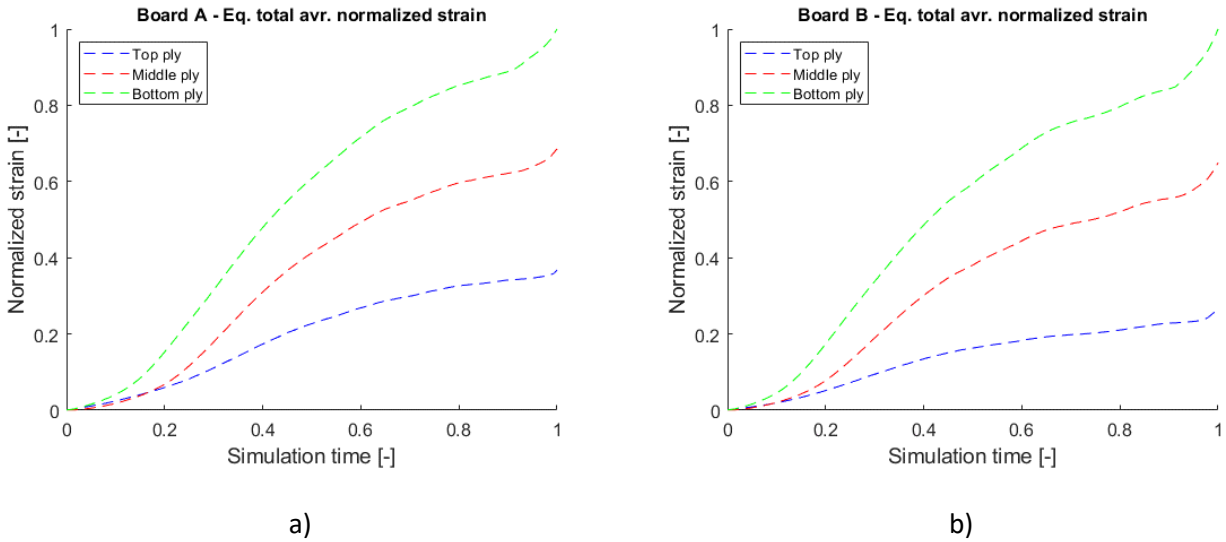

Fig. 14 – The normalized equivalent total average strain over the section. In a) for Board A, and in b) for Board B.

To show the load distributes between the plies we selected to compare the normalized stress levels. Fig. 15 shows the normalized equivalent stress over the section for each ply. For each board, the stresses were normalized by dividing them by the highest stress value occurring, which is the stress in the bottom ply at a load factor (fictitious simulation time) of about 0.8. As seen, the Board B top ply takes a higher part of the load than the Board A top ply, which is natural since, the Board A top ply is more compliant, whilst the Board B top ply is stiffer in comparison to its bottom ply.

The results for the stress distributions are also visible for the failure criteria. In this work, the Tsai-Wu stress criterion (Tsai and Wu 1971) is used for the failure evaluation. The criterion states that the Tsai-Wu index should be below 1 to avoid failure. A detailed discussion about the Tsai-Wu index evaluation can be found in Lindberg and Kulachenko (2021). In Fig. 16, the Tsai-Wu index for each ply for the two boards is plotted. The Tsai-Wu index for the bottom ply is high for both boards. This is due to the high strains occurring in the bottom plies, as previously discussed. Based on these results, we can conclude that the failure initiates in the bottom ply, and that the Tsai-Wu index is higher for Board A than for Board B, which agrees with the observed performances of the considered boards.

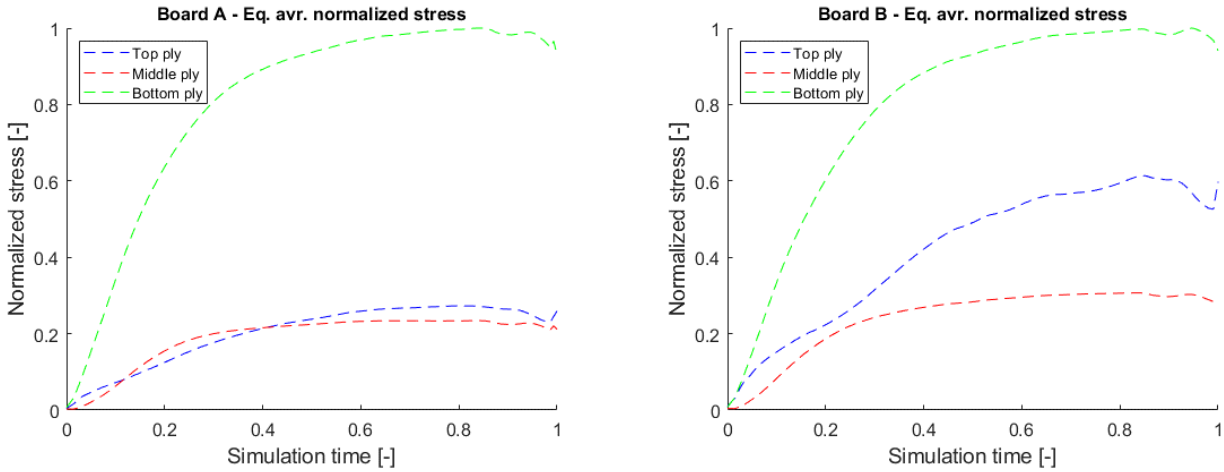

a) b)

439 **Fig. 15** - The normalized equivalent average stress over the section. In a) for Board A, and in b) for Board B.

440
441

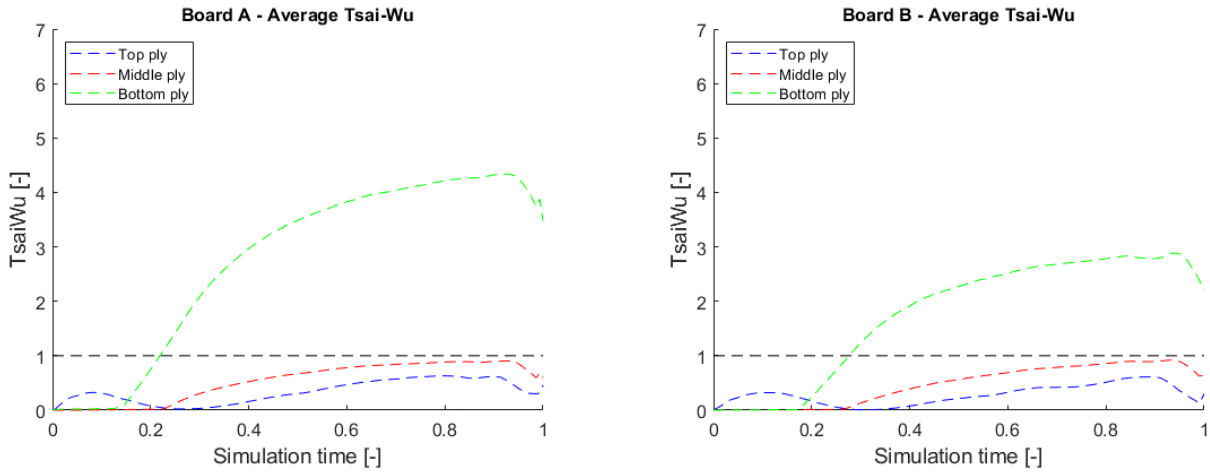

a) b)

442 **Fig. 16** – The average Tsai-Wu index for each ply.

443 To investigate the effect of ply properties on the failure, the stress distribution and the failure criteria
444 were investigated for the case when Board A was placed up-side-down in the tray forming operation.
445 This, in fact, was tested in a pilot test and resulted in a better performance of Board A. In Fig. 17 the
446 outcome of placing Board A up-side-down in the numerical three-ply model is shown. The results are
447 surprising since the top ply and bottom ply end up having the same stress levels. This "unloading" of
448 the bottom ply has a direct impact on the risk of failure, which is seen in Fig. 17b), where the Tsai-Wu
449 index decreases by 60 % as compared to the original case for Board A, see Fig. 16a). This practically
450 implies that due to the high strains in the bottom ply, it is better to have a less stiff ply in the bottom and
451 at the same have a stiffer top ply to take a greater part of the load, hence protecting the bottom ply. In
452 other words, there is an advantage of having the refining energies more balanced than they currently are
453 for Board A.
454

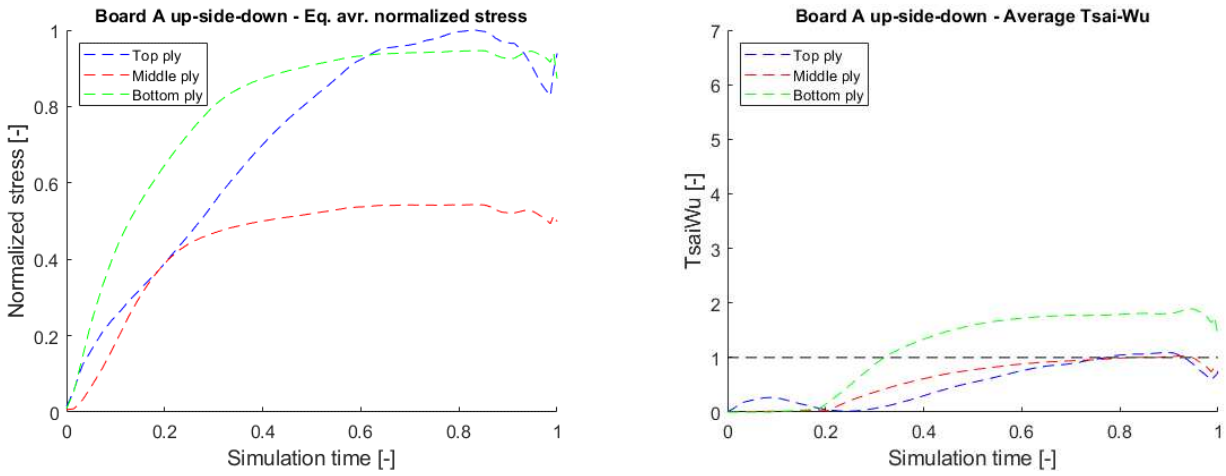

a) b)

Fig. 17 – Results for the case where Board A is placed upside-down. In a) the normalized equivalent stress, and in b) the Tsai-Wu index.

Conclusions

The three-ply FE sub-model used in this project revealed the critical difference between the considered commercial boards when it comes to their performances in the tray forming operation. Although the boards did not show a significant difference in mechanical properties when tested by a conventional method on sheet level, they did show significant discrepancies in mechanical properties when split and tested ply-wise. This difference can solely be explained by dissimilar refining energies used in the constituent pulp.

The results from the three-ply sub-model suggest that the highest strains occur in the bottom ply for both boards, that is, the ply that faces the die. Furthermore, it is seen that the risk of failure increases drastically when the top ply is weakened as the load-bearing function is shifted toward the bottom ply. In fact, with the board having non-uniform strength and stiffness profile through the thickness, it is advantageous to place the weaker side of the board away from the punch in the considered configuration, which is not very intuitive.

The limitation of the study is that the results in the sub-model are directly dependent on the boundary conditions mapped from the model in Lindberg and Kulachenko (2021). As discussed in that study, the model is conservative and does not account for delamination in the creased areas leading to higher strain levels than those encountered in reality. Furthermore, the rate dependency is not considered, and all the material parameters were obtained in the tensile tests performed at a low rate, but the tray forming operation for a 25 mm deep tray takes less than a second. The effect of the tool temperature is not explicitly accounted for. Despite these limitations which prevent accurate estimations of the stress levels, the comparative study clearly shows the importance of including multi-ply structure in simulating converting operations and demonstrates the degrees of freedom which can be used in optimizing the board structure.

Acknowledgements

The authors would like to thank Johan Lindgren, Brita Timmermann, Tommy Ström and Hannes Vomhoff at Holmen Iggesund for their valuable inputs and their support during this study.
The authors are also very grateful to Mossab Alzweighi at KTH Engineering Mechanics for the support with the code used to fit the numerical material models to the experimental tensile tests.

Declarations

Funding

This work has been carried out within the national platform Treesearch and is funded through the strategic innovation program BioInnovation, a joint effort by Vinnova, Formas and the Swedish Energy Agency.

The computations were performed on resources provided by the Swedish National Infrastructure for Computing (SNIC) at HPC2N (projects SNIC 2020/5-428 and SNIC 2021/6-51).

Competing Interests

The authors have no competing interests to declare.

References

Alajami, A., Li, Y., Simon, J. W. (2018) Modelling the anisotropic in-plane and out-of-plane elastic-plastic response of paper. PAMM, 18: e201800322. https://doi.org/10.1002/pamm.201800322

Alzweighi, M., Mansour, R., Tryding, J., Kulachenko, A. (2021) Evaluation of Hoffman and Xia plasticity models against bi-axial tension experiments of planar fiber network materials. International Journal of Solids and Structures: 111358. https://doi.org/10.1016/j.ijsolstr.2021.111358

Awais, M., Sorvari, J., Tanninen, P., Leppänen, T. (2017) Finite element analysis of the press forming process. International Journal of Mechanical Sciences, 131: 767-75. https://doi.org/10.1016/j.ijmecsci.2017.07.053

Baum, G. A., Habeger Jr, C. C., Fleischman Jr, E. H. (1982) Measurement of the orthotropic elastic constants of paper. https://smartech.gatech.edu/bitstream/handle/1853/2848/tps-117.pdf?isAllowed=y&sequence=1

Bedzra, R., Li, Y., Reese, S., Simon, J.-W. (2019) A comparative study of a multi-surface and a non-quadratic plasticity model with application to the in-plane anisotropic elastoplastic modelling of paper and paperboard. Journal of composite materials, 53: 753-67. https://doi.org/10.1177/0021998318790656

Brandberg, A., Kulachenko, A. (2020) Compression failure in dense non-woven fiber networks. Cellulose, 27: 6065-82. https://doi.org/10.1007/s10570-020-03153-2

Chen, F.-K., Lin, S.-Y. (2007) A formability index for the deep drawing of stainless steel rectangular cups. The International Journal of Advanced Manufacturing Technology, 34: 878. https://doi.org/10.1007/s00170-006-0659-3

Fellers, C., de Ruvo, A., Elfstrom, J., Htun, M. (1980) Edgewise compression properties - A comparsion of handsheets made from pulps of various yields. Tappi, 63: 109-12.

Fellers, C., Westerlind, B., De Ruvo, A. (1983) An investigation of the biaxial failure envelope of paper–experimental study and theoretical analysis. In Proceedings of Fundamental Research Symposium, Cambridge, 527-59.

Gill, Y. Q., Jin, J., Song, M. (2020) Comparative study of carbon-based nanofillers for improving the properties of HDPE for potential applications in food tray packaging. Polymers and Polymer Composites, 28: 562-71. https://doi.org/10.1177/0967391119892091

Hagman, A., Nygårds, M. (2012) Investigation of sample-size effects on in-plane tensile testing of paperboard. Nordic Pulp & Paper Research Journal, 27: 295-304. https://doi.org/10.3183/NPPRJ-2012-27-02-p295-304

Hagman, A., Timmermann, B., Nygårds, M., Lundin, A., Barbier, C., Fredlund, M., Östlund, S. (2017) Experimental and numerical verification of 3D forming. In 6th Fundamental Research Symposium, Pembroke College, Oxford, England, 3-26. URL: https://bioresources.cnr.ncsu.edu/resources/experimental-and-numerical-verification-of-3d-forming/

Harrysson, A., Ristinmaa, M. (2008) Large strain elasto-plastic model of paper and corrugated board. International Journal of Solids and Structures, 45: 3334-52. https://doi.org/10.1016/j.ijsolstr.2008.01.031

Hauptmann, M., Wallmeier, M., Erhard, K., Zelm, R., Majschak, J.-P. (2015) The role of material composition, fiber properties and deformation mechanisms in the deep drawing of paperboard. Cellulose, 22: 3377-95. https://doi.org/10.1007/s10570-015-0732-x

545 Hill, R. (1948) A theory of the yielding and plastic flow of anisotropic metals. Proceedings of the Royal
546 Society of London. Series A. Mathematical and Physical Sciences, 193: 281-97.

547 Hristopulos, D. T., Uesaka, T. (2004) Structural disorder effects on the tensile strength distribution of
548 heterogeneous brittle materials with emphasis on fiber networks. Physical Review B, 70:
549 064108. https://doi.org/10.1103/PhysRevB.70.064108

550 Jele, T. B., Lekha, P., Sithole, B. (2021) Role of cellulose nanofibrils in improving the strength properties
551 of paper: a review. Cellulose: 1-27. https://doi.org/10.1007/s10570-021-04294-8

552 Kulachenko, A., Uesaka, T. (2012) Direct simulations of fiber network deformation and failure.
553 Mechanics of materials, 51: 1-14. https://doi.org/10.1016/j.mechmat.2012.03.010

554 Laukala, T., Ovaska, S.-S., Tanninen, P., Pesonen, A., Jordan, J., Backfolk, K. (2019) Influence of pulp
555 type on the three-dimensional thermomechanical convertibility of paperboard. Cellulose, 26:
556 3455-71. https://doi.org/10.1007/s10570-019-02294-3

557 Li, S., Sitnikova, E., Liang, Y., Kaddour, A.-S. (2017) The Tsai-Wu failure criterion rationalised in the
558 context of UD composites. Composites Part A: Applied Science and Manufacturing, 102: 207-
559 17. https://doi.org/10.1016/j.compositesa.2017.08.007

560 Li, Y., Stapleton, S. E., Reese, S., Simon, J.-W. (2016) Anisotropic elastic-plastic deformation of paper:
561 In-plane model. International Journal of Solids and Structures, 100: 286-96.
562 https://doi.org/10.1016/j.ijsolstr.2016.08.024

563 Lindberg, G., Kulachenko, A. (2021) Tray forming operation of paperboard: a case study using implicit
564 finite element analysis. Packaging technology and science, Online.
565 http://doi.org/10.1002/pts.2619

566 Linvill, E., Wallmeier, M., Östlund, S. (2017) A constitutive model for paperboard including wrinkle
567 prediction and post-wrinkle behavior applied to deep drawing. International Journal of Solids
568 and Structures, 117: 143-58. https://doi.org/10.1016/j.ijsolstr.2017.03.029

569 Motamedian, H. R., Halilovic E, A., Kulachenko, A. (2019) Mechanisms of strength and stiffness
570 improvement of paper after PFI refining with a focus on the effect of fines. Cellulose, 26: 4099-
571 124. https://doi.org/10.1007/s10570-019-02349-5

572 Reddy, M. V., Reddy, P. V., Ramanjaneyulu, R. (2019) Effect of heat treatment and sheet thickness on
573 deep drawing formability: a comparative study. International Journal of Applied Engineering
574 Research, 14: 802-05.

575 Rhim, J.-W. (2010) Effect of moisture content on tensile properties of paper-based food packaging
576 materials. Food Science and Biotechnology, 19: 243-47. https://doi.org/10.1007/s10068-010-
577 0034-x

578 Robertsson, K., Borgqvist, E., Wallin, M., Ristinmaa, M., Tryding, J., Giampieri, A., Perego, U. (2018)
579 Efficient and accurate simulation of the packaging forming process. Packaging technology and
580 science, 31: 557-66. https://doi.org/10.1002/pts.2383

581 Rojek, J., Kleiber, M., Piela, A., Stocki, R., Knabel, J. (2004) Deterministic and stochastic analysis of
582 failure in sheet metal forming operations. Steel Grips, 2: 29-34.

583 Scandinavian Pulp, Paper and Board testing committee. SCAN-P 88:01. 2001. Stockholm

584 Siracusa, V., Rocculi, P., Romani, S., Dalla Rosa, M. (2008) Biodegradable polymers for food packaging:
585 a review. Trends in Food Science & Technology, 19: 634-43.
586 https://doi.org/10.1016/j.tifs.2008.07.003

587 Suhling, J., Rowlands, R., Johnson, M., Gunderson, D. (1985) Tensorial strength analysis of paperboard.
588 Experimental mechanics, 25: 75-84. https://doi.org/10.1007/Bf02329129

589 Tjahjanto, D. D., Girlanda, O., Östlund, S. (2015) Anisotropic viscoelastic–viscoplastic continuum model
590 for high-density cellulose-based materials. Journal of the Mechanics and Physics of Solids, 84:
591 1-20. https://doi.org/10.1016/j.jmps.2015.07.002

592 Tsai, S. W. (1984) A survey of macroscopic failure criteria for composite materials. Journal of Reinforced
593 Plastics and Composites, 3: 40-62. https://doi.org/10.1177/073168448400300102

594 Tsai, S. W., Wu, E. M. (1971) A general theory of strength for anisotropic materials. Journal of
595 composite materials, 5: 58-80. https://doi.org/10.1177/002199837100500106

596 Vishtal, A., Retulainen, E. (2012) Deep-drawing of paper and paperboard: The role of material
597 properties. BioResources, 7: 4424-50.

598 Vishtal, A., Retulainen, E., Khakalo, A., Rojas, O. J. (2015) Improving the extensibility of paper:
599 Sequential spray addition of gelatine and agar. Nordic Pulp & Paper Research Journal, 30: 452-
600 60. https://doi.org/10.3183/npprj-2015-30-03-p452-460

601 Wallmeier, M., Linvill, E., Hauptmann, M., Majschak, J.-P., Östlund, S. (2015) Explicit FEM analysis of
602 the deep drawing of paperboard. Mechanics of materials, 89: 202-15.
603 https://doi.org/10.1016/j.mechmat.2015.06.014

604 Wang, J., Wang, L., Gardner, D. J., Shaler, S. M., Cai, Z. (2021) Towards a cellulose-based society:
605 opportunities and challenges. Cellulose: 1-33. https://doi.org/10.1007/s10570-021-03771-4

606 Xia, Q. S., Boyce, M. C., Parks, D. M. (2002) A constitutive model for the anisotropic elastic–plastic
607 deformation of paper and paperboard. International Journal of Solids and Structures, 39: 4053-
608 71. https://doi.org/10.1016/S0020-7683(02)00238-X

609

610

Appendix

A1 - Material model fit for each ply

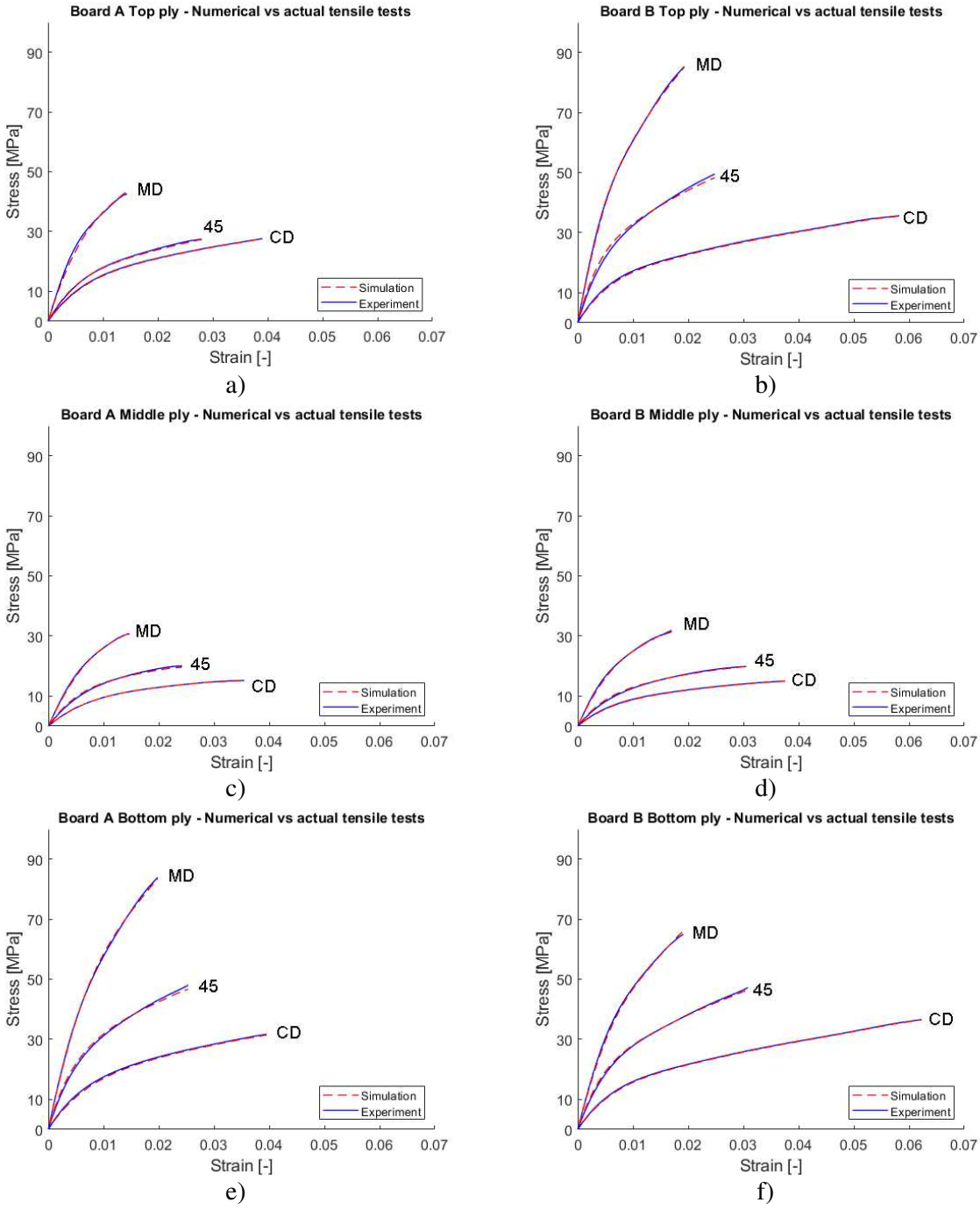

Fig. 18 - – The fitting of the numerical material models to the actual tensile tests for each ply. The failure stress in compression is numerically set to be 50% of that in tension, which is demonstrated in the figures. Note that damage is not included in the model but is instead a part of the post-processing.

621 *A2 - Tensile tests for each ply per direction vs full board*

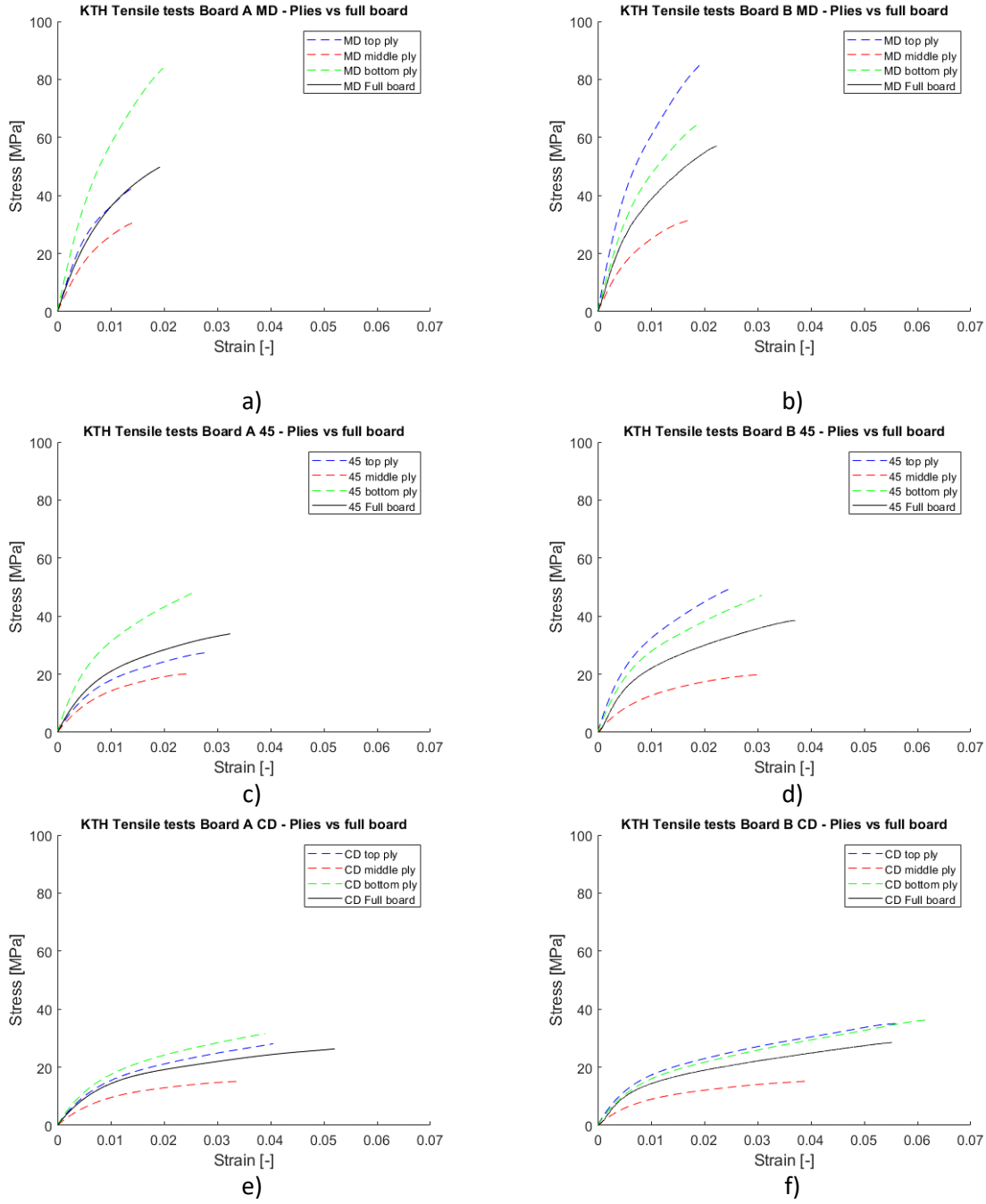

622

623 **Fig. 19 -** Tensile tests per direction: The full paperboards together with the individual plies. As seen, except for
624 the CD direction for Board B (f), the full board has a higher strain to failure than the individual plies. The
625 reasons are discussed in the report.

626

A3-Results from fiber characterization performed by PulpEye

PulpEye is a tool for quantifying the geometric properties of the fibers in the pulp before going into the paperboard machines. It is placed after the complete refining process. The PulpEye at Holmen Iggesund measures the fiber length, projected length (the so-called p-length) and the fiber widths. The p-length is the shortest distance between the ends of each fiber. By using the p-length, the curl index can be computed as (fiber length/p-length) – 1. With the measured data, statistical information about the fibers can be determined, such as the distribution curves and mean values for the fiber length, curl and width.

The mixture for the top and bottom plies is 40% softwood and 60% hardwood. For the middle plies the mixture is different, namely 30% softwood and then 70% reused, so called “broke”, fibers that have been recovered from the spill from the paperboard machine. The broke fibers consist in turn of 50% softwood and 50% hardwood.

The data received for the Board A pulp was measured at a location after that the hardwood and softwood had been refined together. However, the Board B pulp was measured before the softwood and hardwood pulps were mixed, as the pulp extraction after the mixture is not possible. Hence, to get the mixed and final pulp data for the Board B plies, the mixture of the softwood and hardwood pulp had to be done by combining the data files for the individual plies. This was done by taking 40% of the data from the softwood data files, and 60% from the hardwood data files and then creating a new data file which then was used to study the distributions and the mean values of the fiber length, curl and width. This brings some uncertainties about the final data since the weighing of 40% softwood and 60% hardwood in production is based on dry weight, rather than the number of fibers. This could imply that the mean values and the length weighted mean value for the fiber lengths for the Board B plies should be somewhat greater than seen in this report.

In Fig. 20, Fig. 21 and Fig. 22 the results from the PulpEye measurement are shown. Note that, as previously explained, the mixing of the Board B pulp has been done manually for this report by combining 40% of the data from the softwood data file with 60% of the hardwood data file, since no measuring took place with PulpEye on the final pulp going into the machine. Hence the results for the Board B pulp must be interpreted with some cautiousness.

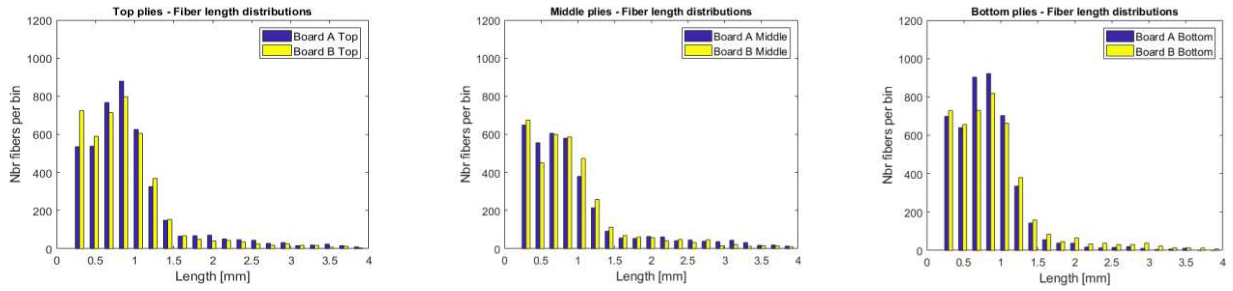

a) b) c)

Fig. 20 - Distribution of the fiber length for the three plies for each paperboard.

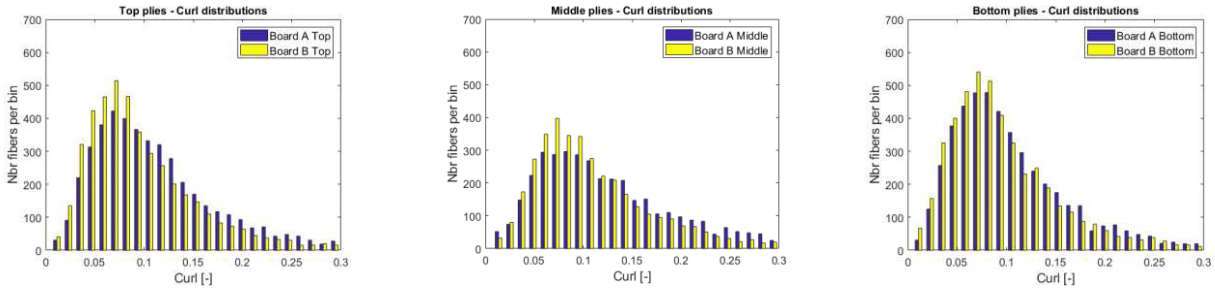

a) b) c)

661 **Fig. 21 -** Distribution of the curl index for the three plies for each paperboard.

662
663

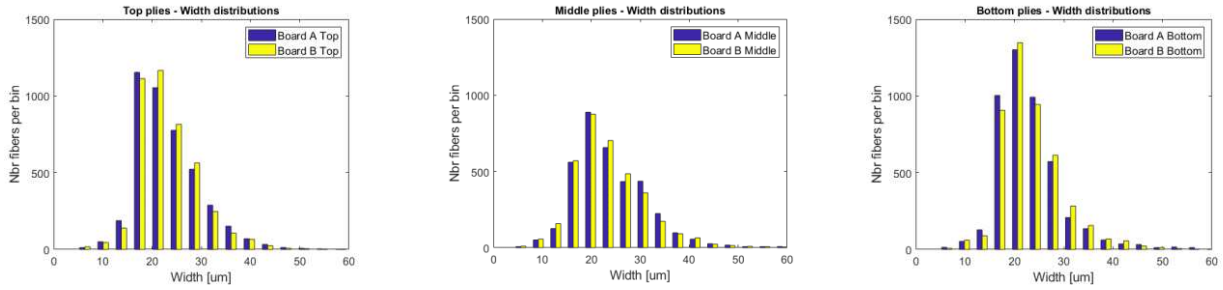

a) b) c)

664 **Fig. 22** - Distribution of the fiber width for the three plies for each paperboard.

665
666
667 The general trend is that the distributions follow each other fairly well. No big deviations are observed.
668 The modes for the fiber length, curl and fiber width are approximately the same for all curves. In Table
669 6 the mean values for the length, curl and width are shown for the top and middle plies. The middle plies
670 are shown in a separate table (Table 7) since they have a different mixture.
671

672 **Table 6** – Mean values from the PulpEye measurements for the top and bottom plies (hardwood/softwood =
673 60%/40%).

Ply	Fiber length: mean [mm]	Fiber length: length weighted mean [mm]	Curl mean [-]	Width mean [um]
Board A Top	0.97	1.43*	0.11	23.2
Board B Top	0.89	1.30	0.10	23.2
Board A Bottom	0.82	1.09**	0.10	22.8
Board B Bottom	0.92	1.35	0.10	23.3

674 *Softwood refiner logged for low energies on several occasions during the time for the measurement.
675 ** Possibly erroneous measurement representing 80%/20% hardwood/softwood rather than 60%/40 %.
676
677
678
679

680 **Table 7** – Mean values from the PulpeEye measurements for the middle plies (hardwood/"broke 50/50" =
681 30%/70%).

Ply	Fiber length: mean [mm]	Fiber length: length weighted mean [mm]	Curl mean [-]	Width mean [um]
Board A Middle	0.98	1.59	0.12	24.1
Board B Middle	0.96	1.48	0.11	23.6

682
683 Even though the data must be interpreted with some cautiousness, the results for the length weighted
684 fiber length mean values are in line with the registered refining energies. The Board A top ply has
685 considerably lower refining energy than for its bottom ply, leading to a somewhat higher length weighted
686 fiber length mean compared to the bottom ply. The bottom ply value, 1.09 mm, is however very low and
687 is closer to an 80%/20% hardwood/softwood combination in the pulp, something discussed in the project
688 team. A more regular 60/40 hardwood/softwood combination should give a value around 1.3 mm for
689 the length weighted fiber length mean.
690
691 The difference in refining energies for Board B also gives a slightly lower length weighted length mean
692 for the top ply compared to the bottom ply. The middle plies show greater values for the length weighted
693 mean, which is partly due to their low refining energies and different mixture.
694
695